Synthesis and characterization of Al-MCM-41 and Al-MCM-48 mesoporous materials

Griselda A. Eimer [a], Liliana B. Pierella [a], Gustavo A. Monti [b], and Oscar A. Anunziata [a,*]

[a] *Grupo de Fisicoquímica de Nuevos Materiales, CITeQ (Centro de Investigación y Tecnología Química), Facultad Regional Córdoba, Universidad Tecnologica Nacional, CC36 – Suc. 16 (5016) Córdoba, Argentina*

[b] *Facultad de Matemática, Astronomía y Física, Universidad Nacional de Córdoba, LANAIS RMS (Fa.M.A.F., UNC-CONICET), (5000) Córdoba, Argentina*

Received 5 September 2001; accepted 21 September 2001

A novel route in the synthesis of Al-MCM-41 and Al-MCM-48, using tetraethoxysilane (TEOS) and sodium aluminate ($NaAlO_2$) as Si and Al source has been obtained. The effect of surfactant nature and the synthesis conditions such as surfactant/Si ratio and hydrothermal treatment time on the formed mesostructure regularity has been studied. Different methods of template removal have also been evaluated. The samples were characterized by X-ray diffraction, nitrogen physisorption, FT-IR, and solid-state MAS NMR spectroscopy.

KEY WORDS: Al-MCM-41; Al-MCM-48; mesoporous materials; M41S; nanostructured materials

1. Introduction

M41S is the collective name for a family of crystalline mesoporous molecular sieves with a regular and well-defined mesopore system. The M41S family is classified into several members: MCM-41 (hexagonal structure), MCM-48 (cubic structure), and other species [1,2]. These materials possess uniform channels and their pore diameter can be varied systematically between 1.5 and 10 nm through the choice of surfactant as the template, auxiliary chemicals, and reaction conditions. MCM-41 consists of a hexagonal array of unidimensional, hexagonally shaped pores. MCM-48 has a three-dimensional, cubic ordered cylindrical pore system and features pore sizes similar to those of MCM-41 when the same template is used during synthesis, but has a smaller synthesis regime than MCM-41. Consequently, MCM-48 has been less studied, even though it should be more applicable as catalyst or adsorbent due to its three-dimensional pore architecture [1–3]. Due to its regular pore structure and pore shape, MCM-41 and MCM-48 have attracted considerable interest as a model substance for sorption of various gases and vapors [4]. These materials with a defined morphology are promising selective adsorbents in separation techniques, *e.g.*, high performance liquid chromatography (HPLC) and supercritical fluid chromatography (SFC) [5,6]. Other interesting physical properties of these materials include a highly specific surface of up to 1000 m^2/g, a specific pore volume of up to 1.3 ml/g and a high thermal stability, all of which make it suitable for many catalytic applications. Therefore, this type of material has potential applications as acidic catalyst for petrochemical processes, in the refining industry in processes requiring moderate acidity and involving bulky molecules, as redox catalysts or as hosts for other chemically active species [7–12]. The incorporation of aluminum and transition metal elements within the silica framework has been implemented in order to increase the acidity, ion exchange capacity and specific catalytic activity of the mesoporous silica molecular sieves. Since the replacement of silicon by aluminum in the framework has been reported [7,13–15], the interest in substituted materials is growing. Tetrahedrally coordinated aluminum ions pave the way for the creation of Brønsted acid sites by the thermal decomposition of ammonium ions generating acidic protons at the Al–O(H)–Si bridges. Brønsted acidity, however, is an essential precondition for a variety of catalytic hydrocarbon reactions. Therefore, attempts to incorporate aluminum into tetrahedral positions of the walls have been intensified [16–19]. There are many reports of synthesis and characterization of Al-MCM-41 with different Si/Al ratios and with different alumina or silica sources, prepared by adding aluminum sources prior to calcination [1–3,15,18–23]. A variety of silica sources have been reported, including sodium silicate and silicon alkoxides. Although the original work by Mobil was performed using a synthetic precipitated silica [1,2] and many groups now favour the use of solid fumed silicas [24], tetraethoxysilane (TEOS) is actually considered to be the most appropriate silica source for the synthesis of MCM-41 and MCM-48 [25–28]. The most often-used aluminum sources are sodium aluminate, aluminum sulphate, aluminum nitrate, pseudoboehmite, and aluminum isopropoxide. Matsumoto *et al.* [29] have reported a route in the synthesis of Al-MCM-41 by hydrolysis of a TEOS–aluminum isopropoxide solution with ammonia as a cata-

* To whom correspondence should be addressed. E-mail: oanunziata@scdt.frc.utn.edu.ar

1011-372X/02/0300-0065/0

lyst. In this case, the hydrolysis and condensation – copolymerization of TEOS and AIP would proceed in the same manner as in the presence of templating surfactant, and give MCM-41 with incorporated aluminum. However, AIP is hydrolyzed more easily than TEOS [30]. Some of the aluminum alkoxides would polymerize themselves and, consequently, the aluminum-containing species would be formed outside the aluminosilicate network of Al-MCM-41. Recently, Cesteros *et al.* [21] studied different factors that affect the final structural integrity of the Al-MCM-41 using δ-Al_2O_3, aluminum sulphate or PHF alumina as the source of Al^{3+} and HiSil-233 or Ludox as silica sources. They reported that the use of Ludox insted of HiSil-233 produces an improvement in the structure after calcination, especially when PHF alumina is used as the alumina source. The sample prepared with aluminum sulphate presented the poorer quality XRD in agreement with the results reported by other authors who used aluminum sulphate for the preparation of Al-MCM-41 [31]. The use of δ-alumina instead of PHF alumina results in an improvement in the structure and a higher amount of tetrahedral aluminum. As can be noted a large variety of silica and aluminum sources has been reported for Al-MCM-41 synthesis but, to our knowledge, there are no reports on the use of TEOS and sodium aluminate together as silica and aluminum sources, respectively. On the other hand, as the MCM-48 mesophase in the conventional synthesis is obtained as an intermediate between the transitions from a hexagonal or disordered mesophase to lamellar mesophases, its formation requires narrow and specific synthesis conditions. Several slightly differing synthesis approaches were explored, *e.g.*, tightly capping the reaction containers or leaving them loosely closed so as to allow for evaporation of the ethanol formed. High quality MCM-48 could only be obtained in autoclaves [28]. Although there are several reports on pure siliceous MCM-48 [2,28,32] we have not found any reports about the synthesis of MCM-48 containing framework aluminum prepared with silica and aluminum sources. In previous works, Anunziata *et al.* [33] studied the synthesis, characterization and catalytic properties of Ti-MCM-41 mesoporous material with TEOS as Si source. In the present study we describe a novel route to prepare aluminosilicates Al-MCM-41 and Al-MCM-48 with both well-defined morphology and high structural ordening, using TEOS and sodium aluminate ($NaAlO_2$) together as silica and aluminum sources, respectively. The influence of surfactant nature as template (dodecyl trimethyl ammonium bromide (DTMABr) or hexadecyl trimethyl ammonium bromide (HTMABr)) and synthesis conditions such as surfactant/Si molar ratio and reaction time on the type of mesophase formed and structure regularity also has been studied. Solid state NMR of ^{27}Al nuclei was used to determine the coordination environment of aluminum species in the mesoporous framework. As it is performed in recent papers, a high resolution FT-IR analysis is discussed in this work to obtain information about the mesostructure framework before and after template removal and identify the presence of silanol groups associated with a characteristic band at 960 cm^{-1}. Moreover, the effect of different post-synthesis treatments for template removal on reticular contraction, structure stability and regularity has been examined.

2. Experimental

The aluminum-containing mesoporous materials (Al-MCM-41 and Al-MCM-48) were prepared as follows: Firstly, TEOS (Aldrich, 98%) and $NaAlO_2$ (Johnson Matthey) were vigorously mixed for 30 min. Then, 25 wt% solution of DTMABr or HTMABr (Aldrich, 99%) in ethanol was dropped under stirring at room temperature. Tetramethylammonium hydroxide 20 wt% aqueous solution (TMAOH) (Merck) was added to the resultant solution and stirring was continued for 5 h. Then, TMAOH and water were further dropped to the milky solution. The mixture was heated at 80 °C for 30 min to remove ethanol used in solution and produced in the hydrolysis of TEOS. The pH of the resultant gel was 11.5. This gel was heated in a static teflon-covered reactor under autogenous pressure at 100 °C for 6–17 days. The final solid reaction product was extracted from the autoclave, filtered, washed with distilled water and dried at 60 °C overnight (as-synthesized MCM). The molar composition of the gels subjected to hydrothermal synthesis was as follows: Si/Al = 20, TMAOH/Si = 0.3, surfactant/Si = 0.15–0.6, water/Si = 60. Different post-synthesis treatments were evaluated to remove the template: (1) Desorption of template under nitrogen atmosphere (5 ml/min) at 500 °C for 6 h and then calcination in air at 500 °C for 6 h. (2) Temperature-programmed desorption (TPD) of template (heating rate of 1 °C/min and N_2 flow of 5 ml/min) to 500 °C also maintaining this temperature for 6 h and further calcination in air at 500 °C for 6 h. (3) Temperature-programmed desorption of template (heating rate of 1 °C/min and N_2 flow of 5 ml/min) to 500 °C maintaining this temperature for 6 h and further temperature-programmed calcination (heating rate of 1 °C/min and air flow of 5 ml/min) to 500 °C also maintaining this temperature for 6 h. For the studies of temperature programming an INSTRELEC programmer was employed, which allows one to change the heat slope. The sodium form of the Al-MCM was characterized by XRD, FT-IR, nitrogen adsorption and solid state MAS NMR spectroscopy. X-ray powder diffraction patterns were collected in air at room temperature on a Rigaku diffractometer using Cu K_α radiation of wavelength 0.15418 nm. Diffraction data were recorded between $2\theta = 1°$ and 10° at an interval of 0.01°. A scanning speed of 2°/min was used. The repetition distance of the pores was obtained by the Bragg law using the position of the first X-ray diffraction line. The lattice parameter a_0 of the hexagonal unit cell can be calculated by $a_0 = (2/\sqrt{3})\, d_{100}$. The pore diameter may be calculated from this value by subtracting 1.0 nm, which is an approximate value for the pore wall thickness usually found in MCM synthesized in a similar procedure. Adsorption–desorption isotherms for

nitrogen, pore size distribution and BET surface area were obtained using a Micromeritics ASAP 2000 instrument. Infrared analysis of the samples was recorded on a JASCO 5300 FT-IR spectrometer either on KBr pellets or on self-supported wafers. The FT-IR spectra in the lattice vibration region were performed using KBr 0.05% wafer technique. In order to determine if the synthesized materials (Na–Al-MCM) contain Si–OH groups, well-defined FT-IR spectra in OH vibration region were made. The samples were pressed into self-supporting wafers (∼8 mg/cm^2), placed in a thermostatized cell with CaF_2 windows connected to a vacuum line and evacuated for 8 h at 400 °C. Solid state NMR experiment was carried out on a Bruker MSL300 spectrometer opertating at a resonance frequency of 78.2 MHz for ^{27}Al. We used a commercial (Bruker) MAS 300WB CP1H-BBWH.VTN-BL4 probe with 4 mm o.d. zirconia rotors. The sample was spun at the magic angle at a rate of 5 kHz. Experiments were carried out at ambient probe temperature (*ca*. 297 K). The ^{27}Al spectrum was recorded using direct polarization with pulses of 2 μs duration and a relaxation delay of 2 s. Aluminum chemical shifts are quoted with respect to 1 M aluminum nitrate solution.

3. Results and discussion

3.1. Al-MCM-41 using DTMABr as template

Al-MCM-41 samples prepared in this study using DTMABr as template are detailed in table 1. These as-synthesized materials were maintained under N_2 atmosphere (5 ml/min) at 500 °C for 6 h to remove the template and then calcined in air at 500 °C for 6 h (post-synthesis treatment 1).

X-ray diffraction patterns of the samples are shown in figure 1 (a) and (b). The Bragg peaks can be indexed as *hkl* reflections of a hexagonal lattice. This diffraction pattern is originated from the regular hexagonal array of uniform channels, characteristic of MCM-41. For the calcined samples, a sharp peak ascribed to the (100) reflection of the hexagonal structure of the mesopores was observed at $2\theta = 2.66°$–$2.70°$, corresponding to $d_{100} = 3.32$–3.27 nm. Besides the strong peak, weak ones ascribed to (110) and (200) reflections at $2\theta = 4.7°$ and $5.4°$, $d = 1.88$ and 1.64 nm, respectively, were observed. The number of well-defined peaks and their relative intensity represent the relative regularity of the MCM-41 structure. Then, the clear peaks shown in figure 1 (a) and (b) indicate that the long-range order structure was achieved [1,2], and the regular mesoporous structure was retained after the introduction of aluminum. No diffraction peaks of other aluminum compounds, such as crystalline alumina and aluminum oxyhydroxide species, were observed. Generally, the FWHH (full width at half-height) of the XRD peaks represents the order of the solid, suggesting that the sample with the narrower FWHH is more ordered. Although mesostructure was formed for the calcined sample I, when the synthesis time increased the FWHH of the XRD peak around $2\theta_{100}$ decreased and the separation of (110) and (200) diffractions became larger to discriminate the hexagonal structure indicating the increasing regularity with synthesis time. After 17 days the pattern typical of the hexagonal structure became prominent (calcined sample II). Moreover, it is well known that surfactant/Si molar ratio is a critical variable in the formation of liquid-crystal templated M41S materials. We observed that the product synthesized with lower template/Si ratio (0.45) had a higher regularity. For this surfactant/Si ratio, we found 10 days hydrothermal treatment is appropiate for the synthesis of MCM-41 with a distinct hexagonal structure (calcined sample III); although 6 days hydrothermal treatment was also enough (calcined sample IV), the intensity of peaks was lower than for sample III. Furthermore, as can be seen in sample II, the (100) Bragg reflection increases sharply in intensity upon removal of the dodecyltrimethylammonium ion template. The d_{100} value decreases from 4.02 to 3.82 nm indicating a lattice contraction upon calcination of 4.98% as is commonly observed, owing to the removal of the surfactant template from the channels, in agreement with the condensation of silanol (SiOH) groups in the walls. All the samples were stable on calcination in air at 500 °C.

Table 1
Characteristics of Al-MCM-41 prepared by using of DTMABr as template

Sample	Synthesis time (days)	Surf/Si	2θ (100) (°)	d_{100} (nm)	a_0 (nm)	Surface area (m^2/g)
I calcined	10	0.60	2.66	3.32	3.84	1504
II as-synthesized	17	0.60	2.54	3.48	4.02	746
II calcined	17	0.60	2.67	3.31	3.82	1598
III calcined	10	0.45	2.70	3.27	3.78	1633
IV calcined	6	0.45	2.70	3.27	3.78	1445

As another method to confirm the highly ordered MCM-41 structure, nitrogen physisorption was carried out for all calcined samples. Adsorption on MCM-41 materials at low relative pressures ($p/p_0 < 0.3$) is accounted for by monolayer adsorption of nitrogen on the walls of the mesopores. As the relative pressure increases ($p/p_0 > 0.3$), the isotherms exhibit sharp inflections characteristic of capillary condensation within uniform mesopores, where the p/p_0 position of the inflection point is related to the diameter of the mesopore. All calcined samples showed type IV adsorption–desorption isotherms according to the IUPAC recommendation, exhibiting the shape characteristic of MCM-41 uniform mesoporous materials [21,22,29]. For p/p_0 between 0.3 and 0.4, a sharp inflection in the isotherms could be observed, indicating the mentionated capillary condensation within uniformly sized mesopores. The sharpness of this step in nitrogen adsorption reflects relative uniformity of the pore size. All the samples showed a narrow uniform pore-size distribution revealing the effectiveness of the synthesis procedure. Calcined sample III exhibited the narrowest pore size distribution according to the highest long-range order whereas calcined sample I showed slightly broader pore size distribution according to a less long-range order. The near coincidence of the two branches of the isotherms can be ascribed to the similar high degree

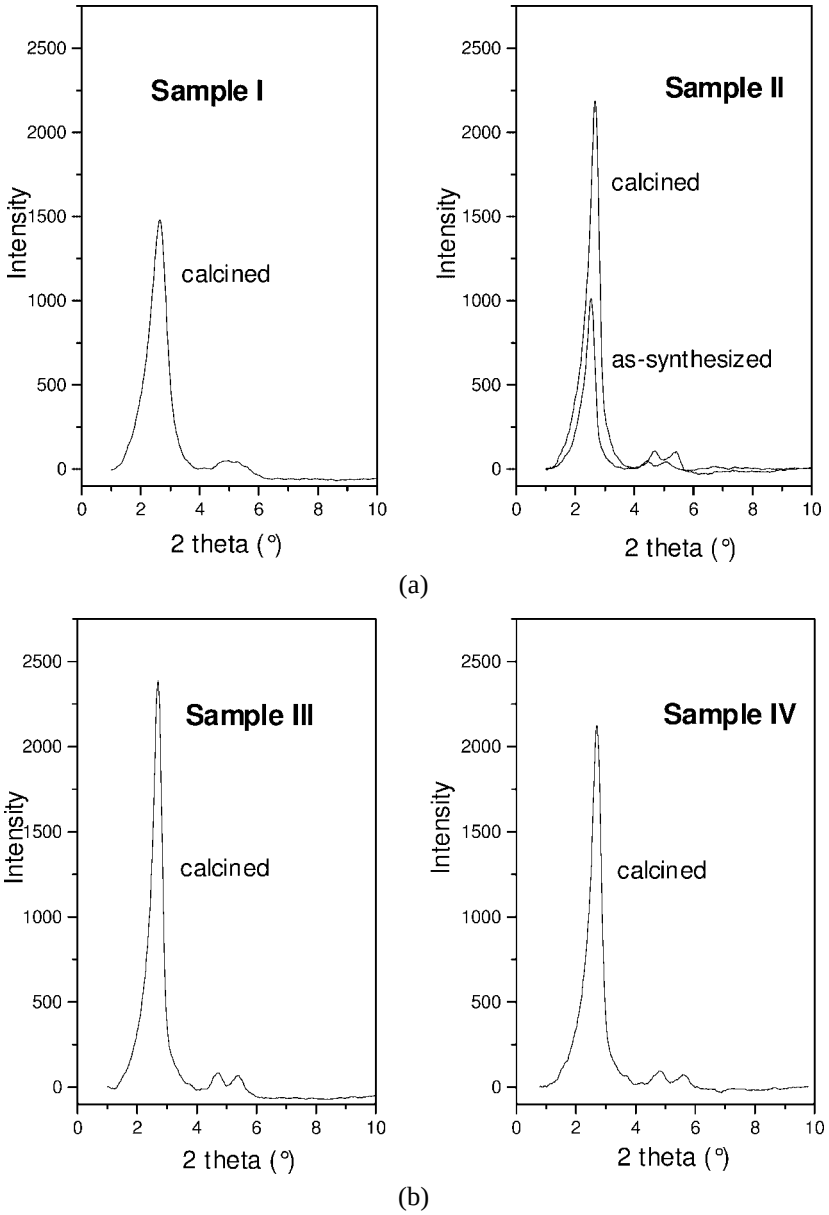

Figure 1. (a) X-ray diffraction patterns of Al-MCM-41 synthesized with DTMABr (samples I and II). (b) X-ray diffraction patterns of Al-MCM-41 synthesized with DTMABr (samples III and IV).

of spontaneity (reversibility) of the adsorption–desorption processes.

Solid-state NMR was used to investigate the local environment of aluminum species after calcining. ^{27}Al NMR may be used to distinguish between tetrahedral and octahedral aluminum coordination to establish the degree of aluminum substitution (tetrahedral sites) in the silica framework. Figure 2 shows the ^{27}Al solid-state MAS NMR spectra of the calcined samples I and III. These spectra exhibit two peaks with shifts of 53 ± 2 and 0 ± 2 ppm. The signal at 53 ± 2 ppm could be assigned to tetrahedrally coordinated framework aluminum (T_d-Al), which was observed in aluminosilicate zeolites [34]. The signal at 0 ± 2 ppm assigned to octahedrally coordinated (O_h-Al) non-framework aluminum [34] would be extra-framework species formed intrinsically during hydrothermal crystallization and/or by

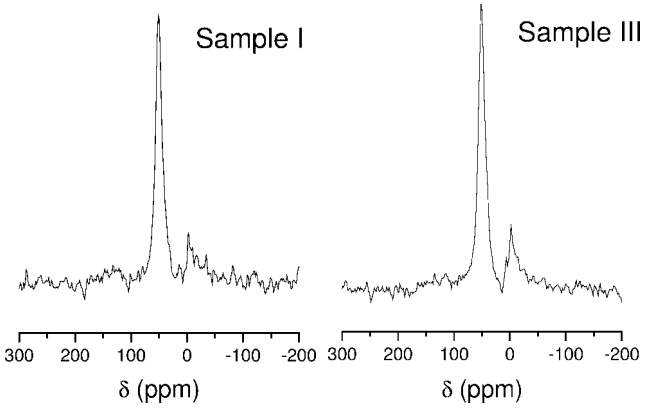

Figure 2. ^{27}Al-MAS NMR spectra of calcined sample I and calcined sample III.

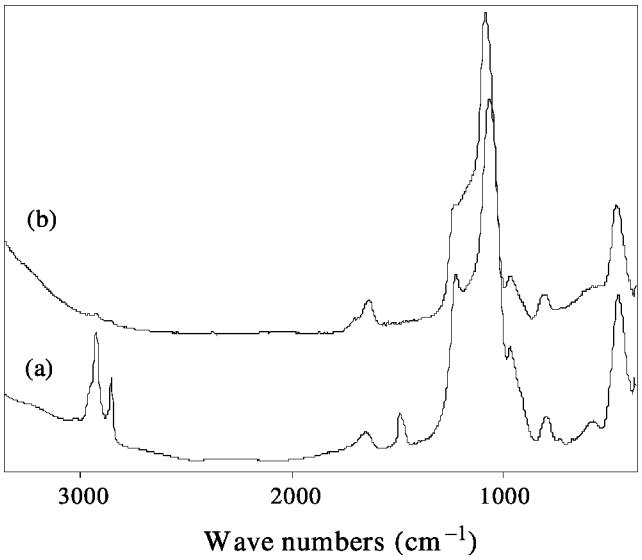

Figure 3. FT-IR spectra in the 400–3400 cm^{-1} range of Al-MCM-41 samples: (a) as-synthesized sample II and (b) calcined sample II.

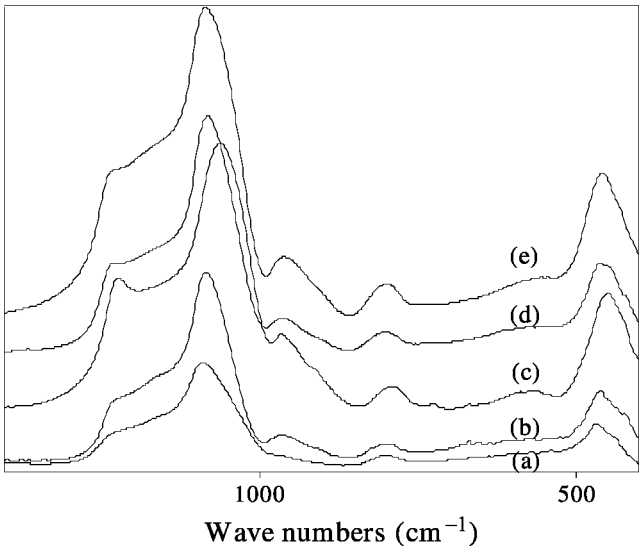

Figure 4. FT-IR spectra in the 400–1400 cm^{-1} range of Al-MCM-41 samples: (a) amorphous sample, (b) calcined sample I, (c) as-synthesized sample II, (d) calcined sample II, and (e) calcined sample III.

dealumination during calcination. Various authors reported that calcination of the as-synthesized Al-MCM-41 to remove the template led to the appearance of octahedrally coordinated extra-framework aluminum species [23,29,35]. Assuming that the concentration of the tetrahedral and octahedral aluminum are proportional to their respective resonances intensities, it can be observed that the peak intensity at 53 ± 2 ppm is much higher than the peak at 0 ± 2 ppm for both samples, indicating that the aluminum was incorporated mainly with tetrahedral coordination in the framework of MCM-41 prepared by the present synthesis procedure, even when a low structural regularity was shown for sample I. The ratio of aluminum in the tetrahedral to that of aluminum in the octahedral environment (Al_{Td}/Al_{Oh}), calculated as a ratio of each peak area, was approximately 1/0.26 for sample III. This result is in agreement with some literature reports [22,29,36] but is in contrast with the results of other authors [21,23], who found that in MCM-41 samples prepared with different aluminum sources the predominant peak was octahedral except for that sample prepared with aluminum sulphate. So, ^{27}Al NMR data of our samples suggest that not only aluminum sulphate as Al source permits the incorporation of Al in the tetrahedral framework position [21,37].

A FT-IR study of the synthesized samples allowed us to identify characteristic bands of the mesoporous framework of Al-MCM-41 before and after template removal. The infrared spectra of the as-synthesized and calcined sample II in the region of 400–3400 cm^{-1} is shown in figure 3. As can be seen, the as-synthesized sample exhibits absorption bands around 2924, 2854, and 1489 cm^{-1} corresponding to asymmetric and symmetric C–H stretching and C–H bending vibrations of the surfactant molecules. Such bands disappear for the calcined sample indicating the total removal of organic material during calcination. Moreover, absorption bands at 1620–1650 cm^{-1} are caused by deformational vibrations of adsorbed water molecules [38]. The framework vibrations region of the infrared spectra (400–1400 cm^{-1}), named the fingerprint zone of the material, is shown in figure 4 for the amorphous sample, as-synthesized sample II and calcined samples I, II, and III. The absorption bands at 1060 and 1223 cm^{-1} in as-synthesized sample II are due to internal and external asymmetric Si–O stretching modes. They are shifted to higher frequencies (1080 and 1229 cm^{-1}, respectively) in calcined sample II. The bands at 790 and 450 cm^{-1} (as-synthesized sample II) are assigned to symmetric Si–O stretching and tetrahedral Si–O bending modes, respectively, and also are slightly shifted to higher frequencies under calcination. Such positive shifts in frequencies would reflect the formation of new Si–O–Si and Si–O–Al bridges during calcination due to an increased network cross-linking [27] and would be accounting for the lattice contraction and structural stabilization that Al-MCM-41 undergoes upon calcination. The decreased relationship between the relative intensity of the 450/790 cm^{-1} bands may be taken as further evidence of the mentioned increased network cross-linking after calcination. Moreover, the band assigned to the external asymmetric Si–O stretching mode is smoothed after calcination according to characteristic spectra of the MCM-41 structure [39,40]. In figure 4, we can observe a sharp band at 960 cm^{-1} for all calcined Al-MCM-41 samples except for the amorphous sample. Several authors have taken FT-IR bands appearing around 960 cm^{-1} in silica-based matrices containing transition metal species as evidence for the isomorphous substitution of Si atoms by heteroatoms because the band was absent in pure silicates [41–44]. Nevertheless, this band already has been observed for crushed silica, silica gels and various high-silica zeolites with a high concentration of defects (*e.g.*, ZSM-34, ZSM-39) [41–51].

In a recent paper, Zhao *et al.* [36] informed that a parent siliceous MCM-41 sample showed two peaks at 810 and 980 cm^{-1} attributed to the symmetrical stretching vibration of Si–O–Si and Si–OH groups, respectively. A Ti-MCM-41 sample also showed the absorption peak at 810 cm^{-1}, whereas the 980 cm^{-1} peak disappeared and a new peak at about 946 cm^{-1} appeared. This band is explained to be due to the formation of Ti–O–Si bridges while the disappearance of the peak at 980 cm^{-1} is explained to be due to the replacement of Si–OH groups by Ti ligands. Perez Pariente *et al.* have observed two weak bands at 999 and 970 cm^{-1} in Beta zeolites with a high Si/Al ratio for which the presence of a high concentration of $Si–O^-$ defects exists and they assigned them to the stretching vibration of $Si–O^-$ groups [52]. Recently, Camblor *et al.* have attributed this band in a Ti-loaded Beta zeolite to Si–OH defects, the concentration of which increases with the incorporation of Ti in the framework position [53]. Dzwigaj *et al.* have assigned this band at 960 cm^{-1} to the presence of vacant T-sites associated with silanol groups generated upon dealuminating in acid medium of the Beta framework [54]. Then, the assignment of such a band at 960 cm^{-1} to the stretching vibration of Si–O vibrators belonging to uncoupled tetrahedral [SiO_4] with a hydroxyl would be more consistent with its appearance in MCM-41 containing aluminum in the framework position. In the case of the as-synthesized Al-MCM-41 (II), two bands appear at 960 and 910 cm^{-1}. Since for the as-synthesized sample, either CTA^+ and/or H^+ can act as counterions for $Si–O^-$ defect groups, the bands at 960 and 910 cm^{-1} can be ascribed to the stretching vibration of Si–O–R ($R = H^+$, CTA^+) groups. Upon calcination, only one IR band ascribed to Si–OH appears at 960 cm^{-1} [51]. Therefore, we have observed that the relationship between the relative intensity of the 960/800 cm^{-1} bands is higher for the materials with higher structural regularity (higher intensity of the (100) Bragg reflection). This feature could be associated with an increase of the typical regular arrangement of the straight one-dimensional and hexagonally shaped channels for MCM-41 and of structural defects caused by the incorporation of Al in the framework. Infrared spectra of calcined samples I, II, and III after heating in vacuum (10^{-5} Torr) at 400 °C for 8 h in the 3900–3300 cm^{-1} range (figure 5) exhibit a band at 3740 cm^{-1} indicating the presence of non-acidic silanol (Si–OH) groups [23,54]. The Si–OH groups concentration is obtained taking account the weight of self-supported wafers. According to the above suggestions samples II and III, which possess more intense (100) Bragg peaks, contain more silanol groups (960 cm^{-1}) than sample I.

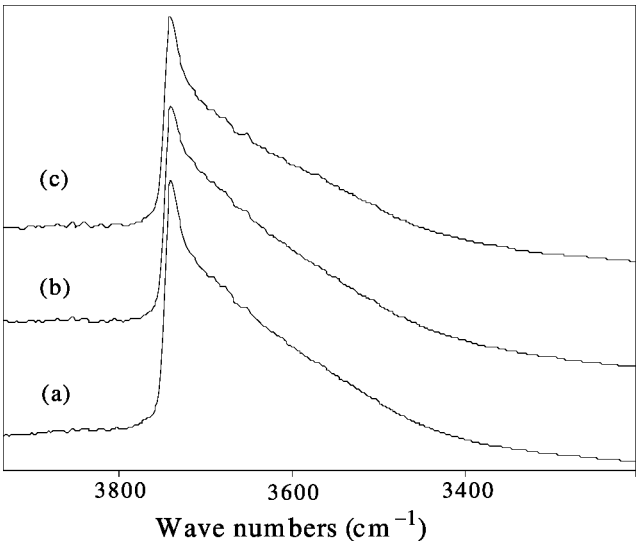

Figure 5. FT-IR spectra of the hydroxy region of Al-MCM-41 samples: (a) calcined sample I, (b) calcined sample II, and (c) calcined sample III.

3.2. Al-MCM-41 and Al-MCM-48 using HTMABr as template

Al-MCM samples prepared in this study using HTMABr as template are detailed in table 2. All the samples were hydrothermally treated for 10 days. The data presented in this table correspond to the as-synthesized materials heated to 500 °C at a rate of 1 °C/min under N_2 flow (5 ml/min), kept at this temperature for 6 h to remove the template and further calcined to 500 °C at a rate of 1 °C/min under air flow (5 ml/min) and kept at this temperature for 6 h (post-synthesis treatment 3).

X-ray diffraction patterns of the samples presented in table 2 are shown in figure 6. As can be seen, when HTMABr is employed as template under the same synthesis conditions used for synthesis of sample III (table 1), a high quality cubic structure appears (sample V). We obtained an XRD pattern for sample V with the diffraction peaks (211) and (220) at 2.46 and 2.82 nm, similar to characteristic diffraction pattern of the cubic member of the M41S family, MCM-48, reported by several authors [1–3,55]. On the other hand, we have also observed that the structure was transformed from cubic into hexagonal with decreasing surf./Si ratio (sample VI). Beck *et al.* [1,2] prepared MCM-41 and MCM-48 by varying the surfactant to silicon mole ratio. They found that the predominant product appeared to be the hexagonal phase, MCM-41, at a $C16H33(CH3)3N^+$/Si ratio of less than 1 and as this ratio increased beyond 1, a cubic phase

Table 2
Characteristics of Al-MCM-48 and Al-MCM-41 prepared with HTMABr as template

Sample	Surf/Si	Structure	2θ (100) (°)	2θ (211) (°)	$d_{(100)}$ (nm)	$d_{(211)}$ (nm)	Surface area (m^2/g)
V calcined[a]	0.45	Cubic	–	2.46	–	3.59	1558
VI calcined[a]	0.3	Hexagonal	2.19	–	4.03	–	1149

[a] Post-synthesis treatment 3.

(MCM-48) could be produced. They also observed that the microscopy and diffraction results for MCM-41 was strikingly similar to those obtained from surfactant/water liquid crystal or micellar phases and proposed a liquid crystal templating (LCT) mechanism for the formation of the M41S materials. This model suggests that the rod-like micelle of surfactant in the water–surfactant liquid phase is piled and silicate addition orders the subsequent silicate-encased micelles. Koyano and Tatsumi [56,57] observed for the synthesis of titanium-containing MCM that the structure was transformed from hexagonal into cubic with increasing concentration of the surfactant, in good agreement with the effect of concentration on the formation of a liquid-crystal phase for the HTMA system [58]. Monnier *et al.* [3] dissented from the mechanism proposed by Beck and coworkers with regard to its insufficient interpretation for establishing the mechanistic understanding needed for better control of the synthesis process. The resemblance, in shape and size, of the surfactant–silicate mesostructure with the corresponding water–surfactant liquid-crystal phase indicates that the interactions responsible for these morphologies are of a similar nature. The governing role of the head-group area (A) in the selection of a particular mesophase has already been recognized in water–surfactant systems: the favored mesophase is that which permits A to be closest to its optimal value A_0, while maintaining favorable packing of the hydrophobic surfactant chain [59]. Monnier *et al.* suggest that in surfactant–silicate systems, the value of A_0 is strongly affected by electrostatic interactions between the silicate and surfactant micelle species. This "charge density matching" establishes a link between the chemical composition and structure of the silicate wall and the formation of a particular structure. The existence of the cubic mesophase is strongly supportive of the important role of such interactions in the formation of surfactant–silicate mesostructures. They proposed a model for mesostructure synthesis, which explained known experimental data as follows: First, multidentate binding of silicate oligomers is formed, which has sufficiently high charge density to permit a lamellar surfactant configuration. Second, the polymerization of the silicate at the surfactant–silicate interface takes place and brings about a diminution of charge density of the larger silicate polyanions, so that A_0 increases. Such diminution of charge density allows the system to increase the average head-group area of the surfactant assembly (A) by adopting a particular mesostructure according to charge density matching criteria. The synthesis mechanism could begin with the hydrolysis and condensation of TEOS [29]. First, the hydrolysis reaction would replace alkoxide groups of TEOS with hydroxyl groups. Second, a proton of the hydroxyl groups would be removed by hydroxyl anion to give silicate anion. Subsequent condensation reactions of terminal silanol ester or silanol groups with silicate anion or aluminate (or silicate–aluminate polyanion in the polymerization process) would produce siloxane bonds. When templating surfactant is present in this system, the interaction between the surfactant molecules and the silicate or aluminosilicate polyanions would result in the formation of hexagonal or cubic mesopore arrays by the mechanism proposed by Monnier *et al.* [3]. This model could account for the formation of the cubic phase as the surfactant nature changes from DTMA into HTMA in the same reaction conditions. Such change would involve a variation of both the average head group area and the ionic strength inducing liquid crystal phase changes to maintain favorable packing of the hydrophobic surfactant chains. Moreover, the transformation from cubic structure into hexagonal structure by changing the surfactant to silicate ratio also supports the above mechanism since this variation in reactant

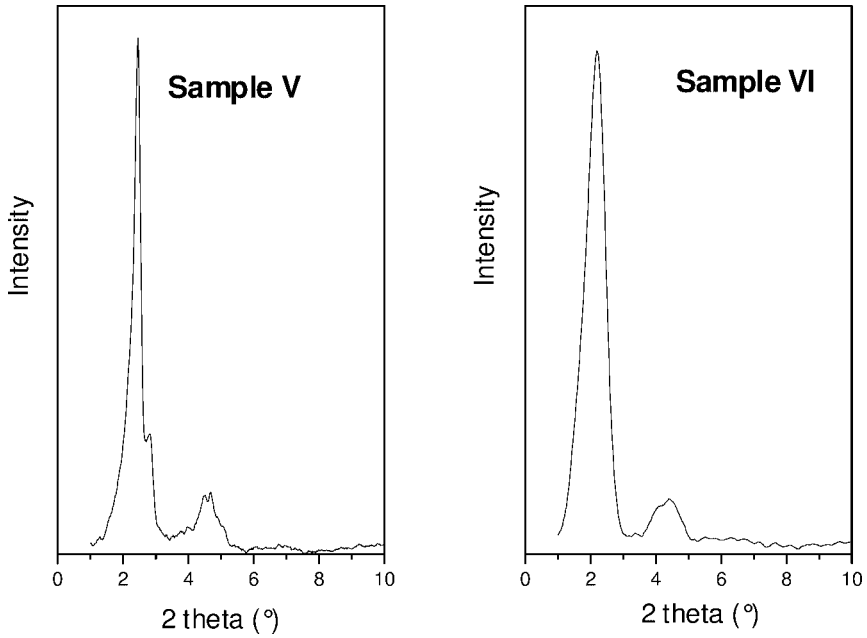

Figure 6. X-ray diffraction patterns of Al-MCM-48 and Al-MCM-41 synthesized with HTMABr (samples V and VI).

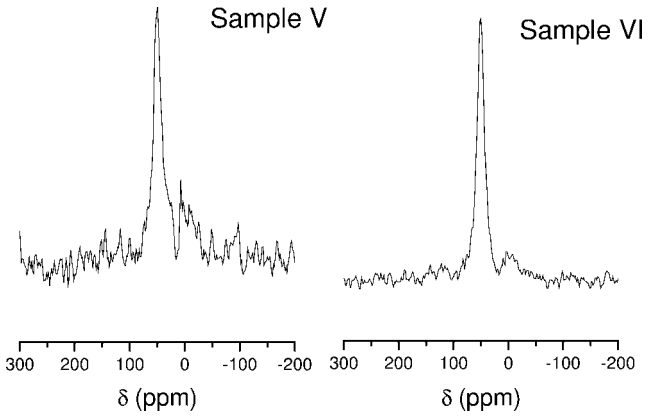

Figure 7. ^{27}Al-MAS NMR spectra of calcined sample V (Al-MCM-48) and calcined sample VI (Al-MCM-41).

composition changes both the surfactant concentration and the ionic strength, either of which can induce liquid crystal phase changes. On the other hand, although the hexagonal mesostructure materials obtained with HTMABr exhibited less regularity than those obtained with DTMABr under similar reaction conditions, we can observ that d_{100} spacing and consequently pore diameter increased with increasing the surfactant chain length, as is expected (tables 1 and 2).

Nitrogen adsorption–desorption isotherms of calcined samples V (MCM-48) and VI (MCM-41) reveal slight differences between these mesoporous supports. Both materials exhibit type-IV isotherms. However the capillary condensation occurs in a more narrow range in MCM-48 than in MCM-41, indicating the existence of more uniform pores in the cubic MCM-48 [28].

As can be seen in NMR spectra of calcined sample V (post-synthesis treatment 3) and calcined sample VI (post-synthesis treatment 3) (figure 7), the peak intensity at 53 ± 2 ppm is much higher than the peak at 0 ± 2 ppm for both samples, indicating that a large portion of the attached aluminum was tetrahedrally coordinated.

XRD patterns of cubic sample V (figure 8): (a) as-synthesized, (b) sample (a) after template desorption under N_2 flow (5 ml/min) at 500 °C for 6 h, and (c) sample (a) after template-thermal-programmed desorption with heating rate of 1 °C/min up to 500 °C and maintaining of this temperature for 6 h under N_2 flow (5 ml/min), show that the template removal produced a reticular contraction which was minor when the thermal-programmed desorption procedure was used. So, this originated a lattice contraction of 2.4% in contrast to procedure without temperature program, which produced a lattice contraction of 3.48%. XRD patterns of cubic sample V (figure 9): (a) after template-thermal-programmed desorption and subsequent calcination in air atmosphere at 500 °C for 6 h (post-synthesis treatment 2) and (b) after template-thermal-programmed desorption and subsequent thermal-programmed calcination with heating rate of 1 °C/min up to 500 °C and maintaining of this temperature for 6 h under air flow (5 ml/min) (post-synthesis treatment 3), indicate again that the calci-

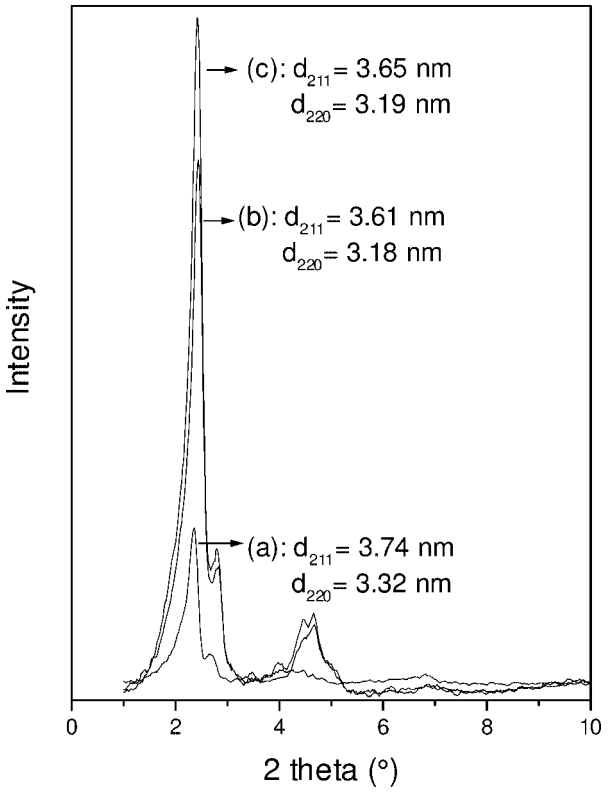

Figure 8. XRD patterns of Al-MCM-48: (a) as-synthesized sample V, (b) sample (a) after template desorption under N_2 flow at 500 °C, and (c) sample (a) after template-thermal-programmed desorption up to 500 °C under N_2 flow.

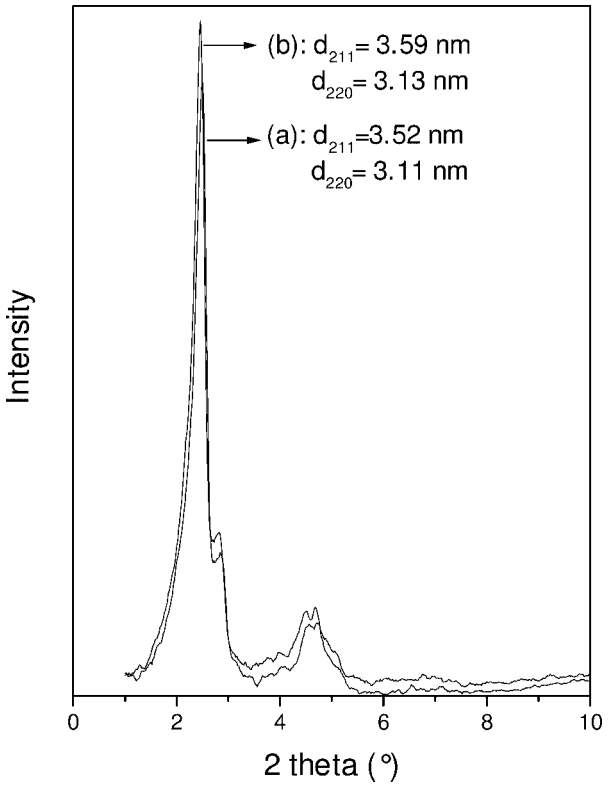

Figure 9. XRD patterns of Al-MCM-48: (a) sample V after post-synthesis treatment 2 and (b) sample V after post-synthesis treatment 3.

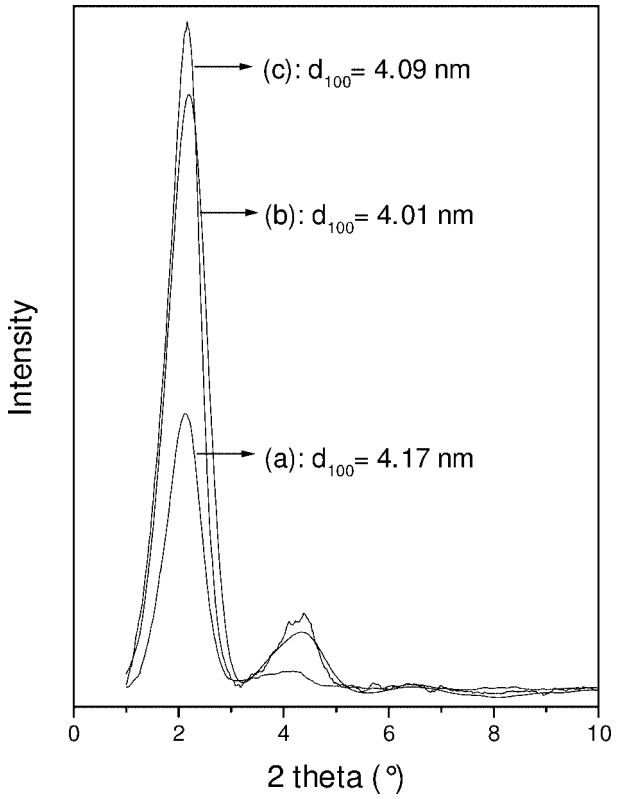

Figure 10. XRD patterns of Al-MCM-41: (a) as-synthesized sample VI, (b) sample (a) after template desorption under N_2 flow at 500 °C, and (c) sample (a) after template-thermal-programmed desorption up to 500 °C under N_2 flow.

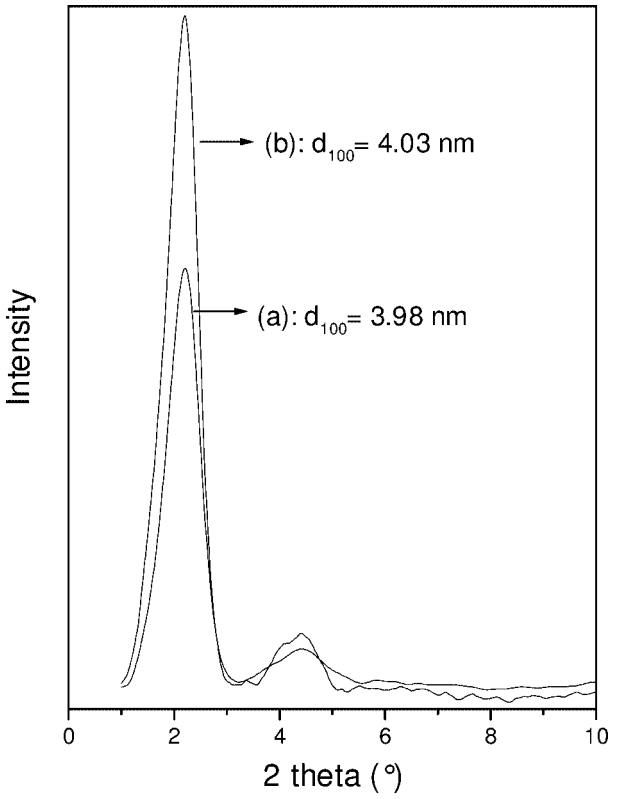

Figure 11. XRD patterns of Al-MCM-41: (a) sample VI after post-synthesis treatment 2 and (b) sample VI after post-synthesis treatment 3.

nation with temperature program and airflow promoted a more minor lattice contraction (minor *d* spacing diminution) than the other proceeding. Furthermore, as can be seen in figures 8 and 9, both template thermal-programmed desorption and thermal-programmed calcination favored the most highly ordered mesostructure. XRD patterns of hexagonal sample VI: (a) as-synthesized, (b) sample (a) after template desorption under N_2 flow (5 ml/min) at 500 °C for 6 h, and (c) sample (a) after template-thermal-programmed desorption with heating rate of 1 °C/min up to 500 °C and maintaining of this temperature for 6 h under N_2 flow (5 ml/min) shown in figure 10 and XRD patterns of hexagonal sample VI: (a) after post-synthesis treatment 2 and (b) after post-synthesis treatment 3 shown in figure 11, suggest that both the template removal using hexadecyltrimethylammonium thermal-programmed desorption and the thermal-programmed calcination of the cubic samples produced also minor lattice contractions in the mesostructure framework and long-range ordered structure.

The infrared spectra of the samples: (a) as-synthesized sample V, (b) sample (a) after post-synthesis treatment 3, (c) as-synthesized sample VI, and (d) sample (c) after post-synthesis treatment 3, in the fingerprint region of material (400–1400 cm^{-1}) (figure 12), present the same absorption bands characteristic of the MCM-structure observed for samples synthesized with DTMABr. The assignment of these bands is according to that given for figure 3 and the positive shifts in frequencies of bands assigned to Si–O stretching and bending modes upon calcination were also observed. As can be seen, there are no differences between the MCM-41 and MCM-48 spectrum; then FT-IR analysis is unable to discriminate the

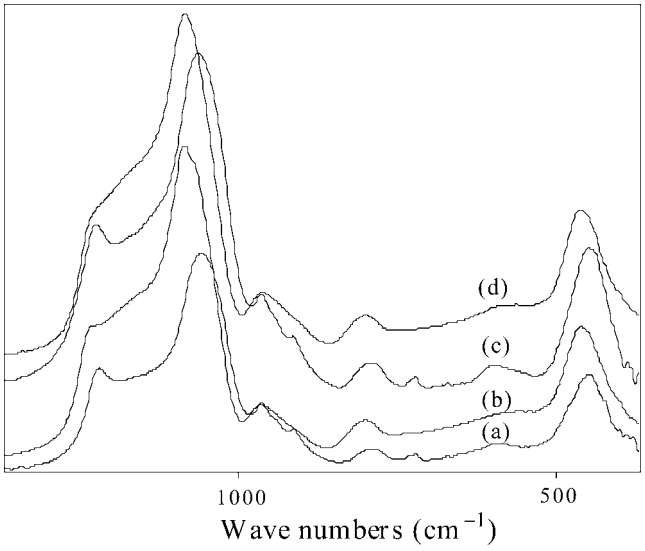

Figure 12. FT-IR spectra in the 400–1400 cm^{-1} range of Al-MCM-48 and Al-MCM-41 samples: (a) as-synthesized sample V, (b) sample (a) after post-synthesis treatment 3, (c) as-synthesized sample VI, and (d) sample (c) after post-synthesis treatment 3.

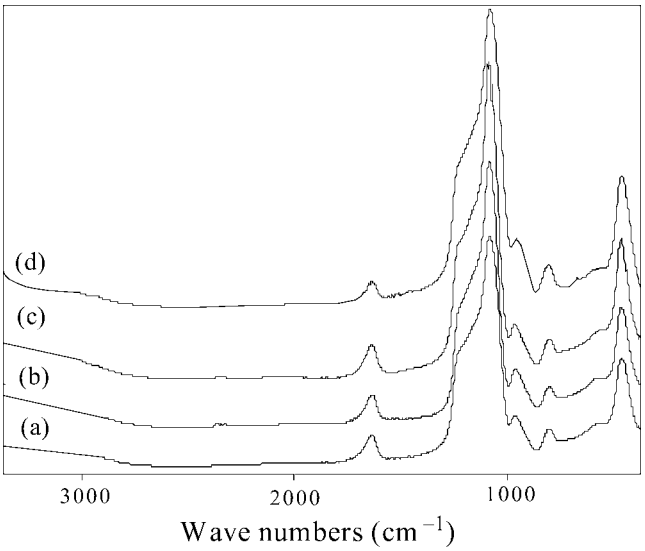

Figure 13. FT-IR spectra in the 400–3400 cm^{-1} range of Al-MCM-48 samples: (a) sample V after template desorption at 500 °C under N_2 flow, (b) sample V after template-thermal-programmed desorption up to 500 °C under N_2 flow, (c) sample V after post-synthesis treatment 2, and (d) sample V after post-synthesis treatment 3.

hexagonal structure from the cubic one. In addition, remarkable differences between the MCM-41 spectra obtained with DTMABr and HTMABr were not noted. Figure 13 shows the infrared spectra of the following samples in the 3400–400 cm^{-1} range: (a) sample V after template desorption at 500 °C for 6 h under N_2 flow, (b) sample V after template-thermal-programmed desorption with heating rate of 1 °C/min up to 500 °C and maintaining of this temperature for 6 h, under N_2 flow, (c) sample V after template-thermal-programmed desorption and calcination in air at 500 °C (post-synthesis treatment 2), and (d) sample V after template-thermal-programmed desorption and thermal-programmed calcination up to 500 °C under air flow (post-synthesis treatment 3). No shifts in frequencies of bands were observed between the samples subjected to different thermal treatments and the absorption bands due to surfactant molecules did not appear in either of the spectra indicating the total removal of the template under all the thermal treatments.

4. Conclusions

Al-MCM-41 and Al-MCM-48 molecular sieves with a Si/Al ratio of 20 can be prepared by hydrothermal synthesis using $NaAlO_2$ and TEOS as aluminum and silica sources, respectively. This route of synthesis enabled us to access mesoporous materials with high regularity and the particular mesostructure was intimately linked to the surfactant nature (DTMABr or HTMABr) and the synthesis conditions such as the hydrothermal treatment time and template/Si ratio. MCM-41 obtained with DTMABr showed well-defined diffraction patterns and its regularity increased with increasing synthesis time and decreasing surfactant/Si ratio. A cubic phase appeared when HTMABr was used instead of DTMABr under the same reaction conditions and it is transformed into a hexagonal one by decreasing the surfactant/Si ratio. Such transformations can be explained through both the formation of a liquid crystal phase for the surfactant systems and the Monnier *et al.* [3] model for the synthesis of the M41S materials. The aluminum atom was tetrahedrally incorporated into the silica framework mesoporous structure. A FT-IR study allowed us to obtain information about the mesostructure framework before and after template removal and identify the presence of silanol groups associated with a characteristic band at 960 cm^{-1}. Thus, template thermal-programmed desorption and thermal-programmed calcination procedures allowed us to achieve the smallest lattice contraction after the surfactant elimination.

Acknowledgment

OAA and LBP, Conicet Reserchers; GAE and GAM, Conicet Posdoctoral Fellowships. The authors are grateful to Agencia Córdoba Ciencia of Argentina for financial support.

References

[1] C. Kresge, M. Leonowicz, W. Roth, J. Vartuli and J. Beck, Nature 359 (1992) 710.
[2] J. Beck, J. Vartuli, W. Roth, M. Leonowicz, C. Kresge, K. Schmitt, C. Chu, D. Olson, E. Sheppard, S. McCullen, J. Higgins and J. Schlenker, J. Am. Chem. Soc. 114 (1992) 10834.
[3] A. Monnier, F. Schuth, Q. Huo, D. Kumar, D. Margolese, R. Maxwell, G. Stucky, M. Krishnamurty, P. Petroff, A. Firouzi, M. Janicke and B. Chmelka, Science 261 (1993) 1299.
[4] R. Schmidt, M. Stocker, E. Hansen, D. Akporiaye and O. Ellestad, Micropor. Mater. 3 (1995) 443.
[5] M. Grun, A. Kurganov, S. Schacht, F. Schuth and K. Unger, J. Chromatogr. A 740 (1996) 1.
[6] M. Grun, I. Lauer and K. Unger, Adv. Mater. 9 (1997) 254.
[7] A. Corma, V. Fornes, M. Navarro and J. Perez Pariente, J. Catal. 148 (1994) 569.
[8] S. Morin, P. Ayrault, E. el Mouahid, N. Gnep and M. Guisnet, Appl. Catal. A 159 (1997) 317.
[9] A. Corma, Chem. Rev. 97 (1997) 2373.
[10] M. Climent, A. Corma, R. Guil-Lopez, S. Iborra and J. Primo, J. Catal. 175 (1998) 70.
[11] K. Kloetstra and H. Van Bekkum, J. Chem. Soc. Chem. Commun. (1995) 1005.
[12] K. Moller and T. Bein, Chem. Mater. 10 (1998) 2950.
[13] W. Kolodzieski, A. Corma, M. Navarro and J. Perez Pariente, Solid State Nuc. Magn. Reson. 2 (1993) 17.
[14] P. Tanev, M. Chibwe and T. Pinnavaia, Nature 368 (1994) 321.
[15] R. Schmidt, D. Akporiaye, M. Stocker and O. Ellestad, J. Chem. Soc. Chem. Commun. (1994) 1493.
[16] K. Busio, J. Janchen and J. van Hooff, Micropor. Mater. 5 (1995) 211.
[17] A. Tuel and S. Gontier, Chem. Mater. 8 (1996) 114.
[18] Y. Sun, Y. Yue and Z. Gao, Appl. Catal. A 161 (1997) 121.
[19] H. Kosslick, G. Lischke, B. Paelitz, W. Storek and R. Fricke, Appl. Catal. A 184 (1999) 49.
[20] S. Bagshaw and F. Testa, Micropor. Mesopor. Mater. 39 (2000) 67.
[21] Y. Cesteros and G. Haller, Micropor. Mesopor. Mater. 43 (2000) 171.
[22] B. Lindlar, A. Kogelbauer and R. Prins, Micropor. Mesopor. Mater. 38 (2000) 167.
[23] B. Chakraborty and B. Viswanathan, Catal. Today 49 (1999) 253.

[24] A. Sayari, Y. Yang, M. Kruk and M. Jaroniec, J. Phys. Chem. B 103 (1999) 3651.
[25] Q. Cai, W. Lin, F. Xiao, W. Pang, X. Chen and B. Zou, Micropor. Mesopor. Mater. 32 (1999) 1.
[26] G. Oye, J. Sjoblom and M. Stocker, Micropor. Mesopor. Mater. 34 (2000) 291.
[27] M.V. Landau, S.P. Varkey, M. Herskowitz, O. Regev, S. Pevzner, T. Sen and Z. Luz, Micropor. Mesopor. Mater. 33 (1999) 149.
[28] K. Moller, T. Bein and R. Fischer, Chem. Mater. 10 (1998) 1841.
[29] A. Matsumoto, H. Chen, K. Tsutsumi and M. Grun, Micropor. Mesopor. Mater. 32 (1999) 55.
[30] S. Sakka, Sol–Gel Hou no Kagaku (Science of Sol-Gel Method) (Agune-Shoufu Sha, Tokyo, 1988) ch. 3.
[31] Z. Luan, C. Cheng, W. Zhou and J. Klinowski, J. Phys. Chem. 99 (1995) 1018.
[32] S. Jun, J. Kim, R. Ryoo, Y. Soo and M. Han, Micropor. Mesopor. Mater. 41 (2000) 119.
[33] O. Anunziata, L. Pierella, F. Requejo and E. Lede, in: *2nd Int. Symp. Mesopor. Mol. Sieves*, Canada (2000).
[34] G. Engelhardt, Stud. Surf. Sci. Catal. 58 (1991) 285.
[35] H. Kosslick, G. Lischke, G. Walther, W. Stoek, A. Martin and R. Fricke, Micropor. Mater. 9 (1997) 13.
[36] X. Zhao, G. Lu and X. Hu, Micropor. Mesopor. Mater. 41 (2000) 37.
[37] Z. Luan, C. Cheng, W. Zhou and J. Klinowski, J. Phys. Chem. 99 (1995) 1018.
[38] A.V. Kiselev and V.I. Lygin, *Infrared Spectra of Surface Compounds and Adsorbed Substances* (Nauka, Moscow, 1972).
[39] A. Liepold, K. Roos, W. Reschetilowski, A. Esculcas and J. Rocha, J. Chem. Soc. Faraday Trans. 92 (22) (1996) 4623.
[40] C.H. Rhee and J.S. Lee, Catal. Today 38 (1997) 213.
[41] T. Sen, P.R. Rajamohanan, S. Ganapathy and S. Sivasanker, J. Catal. 163 (1996) 354.
[42] A. Tuel and Y.B. Taarit, Appl. Catal. 102 (1993) 201.
[43] S.H. Chien, J.C. Ho and S.S. Mon, Zeolites 18 (1997) 182.
[44] K. Unger, in: *Adv. Chem. Series* 2341994, ed. M.J. Comstock (Washington, DC) 168.
[45] M. Decottignies, J. Phalippou and J. Zarzycki, J. Mater. Sci. 13 (1978) 2605.
[46] R. Soda, Bull. Chem. Soc. Jpn. 34 (1961) 1491.
[47] A. Duran, C. Serna, V. Fornes and J.M. Fernández-Navarro, J. Non-Cryst. Solids 82 (1986) 69.
[48] M. Hino and T. Sato, Bull. Chem. Soc. Jpn. 44 (1971) 33.
[49] M. Ocana, V. Fornes and C.J. Serna, J. Non-Cryst. Solids 107 (1989) 187.
[50] P. Jacobs and J. Martens, Stud. Surf. Sci. Catal. 33 (1987) 1.
[51] M.A. Camblor, A. Corma and J. Perez Pariente, J. Chem. Soc. Chem. Commun. (1993) 557.
[52] J. Perez Pariente, J. Sanz, V. Fornes and A. Corma, J. Catal. 124 (1990) 217.
[53] M.A. Camblor, M. Constantini, A. Corma, L. Gilbert, P. Esteve, A. Martinez and S. Valencia, J. Chem. Soc. Chem. Commun. (1996) 1339.
[54] S. Dzwigaj, P. Massiani, A. Davidson and M. Che, J. Mol. Catal. A 155 (2000) 169.
[55] J. Vartuli, K. Schmith, C. Kresge, W. Roth, M. Leonowicz, S. McCullen, S. Hellring, J. Beck, J. Schlencker, D. Olson and E. Sheppard, Chem. Mater. 6 (1994) 2317.
[56] K. Koyano and T. Tatsumi, Chem. Commun. (1996) 145.
[57] K. Koyano and T. Tatsumi, Micropor. Mater. 10 (1997) 259.
[58] P. Vinson, J. Bellare, H. Davis, W. Miller and L. Scriven, J. Colloid Interface Sci. 142 (1991) 74.
[59] J. Charvolin and J. Sadoc, J. Phys. 48 (1987) 1559.